Materials Letters: X 5 (2020) 100034

Contents lists available at ScienceDirect

Materials Letters: X

journal homepage: www.elsevier.com/locate/mlblux

Fe/SBA-15: Characterization and its application to a heterogeneous solar photo-Fenton process in order to decolorize and mineralize an azo dye

J.J. Arroyo-Gómez [a,1], C.F. Toncón-Leal [a,1], A.J. dos Santos [b,*,1], M.S. Moreno [c], K. Sapag [a], C.A. Martínez-Huitle [b,d,*]

[a] Laboratorio de Sólidos Porosos (LabSoP), Infap-Conicet, Universidad Nacional de San Luis, Av. Ejército de los Andes 950, 5700 San Luis, Argentina
[b] Laboratório de Eletroquímica Ambiental e Aplicada (LEAA), Instituto de Química, Universidade Federal do Rio Grande do Norte, P59072-970 Natal, Brazil
[c] Centro Atómico Bariloche, 8400 San Carlos de Bariloche, Argentina
[d] National Institute for Alternative Technologies of Detection, Toxicological Evaluation and Removal of Micropollutants and Radioactives (INCT-DATREM), Institute of Chemistry, UNESP, P.O. Box 355, 14800 900 Araraquara, SP, Brazil

ARTICLE INFO

Article history:
Received 12 June 2019
Received in revised form 1 December 2019
Accepted 9 December 2019
Available online 20 December 2019

Keywords:
Mesoporous silica
Advanced oxidation process
Azo dye

ABSTRACT

Fe/SBA-15 catalyst with different iron (Fe) loads (6% and 10% wt.) was synthesized via incipient wetness impregnation. The potential photocatalytic properties were tested using solar radiation, as a novel catalyst in heterogeneous Fenton approach to degrade Methyl Orange azo dye. A partial pore blocking of the substrate by Fe nanoparticles was detected and the main form of Fe present was Fe_2O_3. When the Fe (10%)/SBA-15 catalyst was used for heterogeneous solar photo-Fenton reaction, total discoloration of the effluent was achieved in 90 min, and 89% of COD was removed in 240 min. Short-chain linear carboxylic acids were followed over time, as well as inorganic ions.

1. Introduction

Advanced oxidation processes (AOPs) have received special attention because of their capability to remove recalcitrant organic pollutants. Among them, Fenton's process is one of the most efficient used in wastewater treatment. This process is divided into homogeneous and heterogeneous, depending on the physical state of the iron catalyst. The latter involves the reaction between Fe-based solid catalyst and the H_2O_2 to generate hydroxyl radicals (·OH), which are highly reactive species, with high oxidation power (E^0 = 2.80 V) [1,2]. The solar photo-Fenton is an environmentally friendly and cost-effective process [3], since sunlight is a renewable and free source of UV radiation that could be used to produce extra ·OH [4]. Regarding the catalyst, the use of mesoporous supports, such as SBA-15, can improve metal loading, dispersion, and consequently, the catalytic performance due to their higher specific surface area [5]. Also, the use of a support with ordered porosity allows a better diffusion to and from the active sites [6]. Finally, it has been reported that metallic nanoparticles supported on porous materials present a higher catalytic activity towards the decomposition of organic pollutants via Fenton reactions [5–8]. For this reason, in this work, we studied Fe supported on SBA-15 as catalyst with different iron loads in heterogeneous Fenton reaction and for the first time, in heterogeneous solar photo-Fenton (HSPF) to degrade Methyl Orange azo dye.

2. Material and methods

2.1. Catalysts preparation

A solution of $Fe(NO_3)_3{\cdot}9H_2O$ in ethanol was added to the support (SBA-15). Afterwards, the solvent was removed and the resulting product was calcined at 300 °C for 2 h (details in Supplementary Material Information (SM).

2.2. HSPF procedure

Fe/SBA-15 (0.05 g) catalyst was disperse in 100 mL of 20 mg L^{-1} Methyl Orange azo dye (MO, Sigma-Aldrich). Afterwards, the solution was acidified with 1.0 M H_2SO_4 for pH 3.0 and 10 mM H_2O_2 was added. HSPF process was performed on sunny days of October 2018 in Natal/RN, Brazil, using the apparatus described by Batista et al. 2017 [4]. The average of the natural UV irradiance was about of 35.8 W m^{-2}. The color removal of the solution was followed

* Corresponding authors at: Laboratório de Eletroquímica Ambiental e Aplicada (LEAA), Instituto de Química, Universidade Federal do Rio Grande do Norte, P59072-970 Natal, Brazil (C.A. Martínez-Huitle).
E-mail addresses: alexsandrojhones@hotmail.com (A.J. dos Santos), carlosmh@quimica.ufrn.br (C.A. Martínez-Huitle).
[1] These authors contributed equally to this work.

https://doi.org/10.1016/j.mlblux.2019.100034
2590-1508/

with an UV–vis spectrophotometer Analytikjena SPECORD 210 PLUS at λ_{max} = 465 nm, the maximum wavelength of the dye (more details in SM).

3. Results and discussion

3.1. Fe/SBA-15 characterization

Characterization analysis for Fe(6%)/SBA-15 and Fe(10%)/SBA-15 were performed, but only Fe(10%)/SBA-15 results are presented in this communication because it showed better performance for environmental applications. XRF analysis of the catalyst indicated an iron loading of 5.4% and 9.5%, respectively, indicating that the synthesis method was effective to modify the substrate with the desired iron load. SEM micrographs of both SBA-15 and Fe/SBA-15 show a uniform and homogeneous surface as well as forming elongated arrays (Fig. 1a and 1b). TEM micrographs (Fig. 1c and d) reveal that these arrays possess a hexagonal shape with ordered cylindrical pores. Fig. 1d clearly shows how the metal particles are dispersed within the pores, with a non-uniform distribution. In some cases, the pores of the SBA-15 support were partially blocked. N_2 adsorption–desorption isotherm (Fig. 2a) for SBA-15 was of type IV(a) with an H1 hysteresis loop [9], which is characteristic of materials with narrow-sized cylindrical mesopores [10]. After the incorporation of iron, the isotherm shape remained unchanged; however, the hysteresis loop changes to H5, which corresponds to materials with open and partially blocked mesopores [11]. The pore size distribution (PSD) of the pristine and Fe (10%)/SBA-15 (Fig. 2b) showed that the predominant pore volume was in the mesoporous zone (2–50 nm), presenting also lower micropores volume ($\leq$20 nm). In both materials, the PSD presented a unimodal distribution, where the differences between them can be attributed to the incrustation of iron oxide inside the pores in the support. Table 1 displays the main textual properties of the materials, the reduction in specific surface area (S_{BET}), total pore volume (V_{TP}), and primary mesopore volume (V_{MPP}) related to the fact that the nanoparticles are deposited in the mesochannels. There was no change in the micropore volume ($V_{\mu P}$). In Fig. SM1-a, low angle X-ray diffractograms for SBA-15 and Fe(10%)/SBA-15 are shown, and the diffraction peaks of the planes (1 0 0), (1 1 0), and (2 0 0), characteristic of the hexagonal array of materials with primary mesopores [12], are clearly observed, consistently with the TEM results. At high angles of the Fe(10%)/SBA-15 sample, Fig. SM1-b showed the typical diffractogram of amorphous silica of SBA-15, consisting of a reflection at 2θ ca. 24. It also showed broadened reflections of Fe_2O_3 with low intensity peaks, which suggest small crystal size. The latter may imply the presence of nanometric iron oxide over the substrate surface (out and inside the pores). The general XPS spectra (see, SM2) of the samples revealed the presence of Si, and O; and Si, O, and Fe, for the SBA-15 and Fe(10%)/SBA-15, respectively. For the Fe(10%)/SBA-15, in the Fe 2p spectrum (Fig. SM1-c), the peaks appears at 724.1 eV and 710.5 eV (Δ = 13.6 eV), which corresponds to Fe $2p_{1/2}$ and $2p_{3/2}$. Finally, the position and shape of the iron peaks suggested that is present in form of oxide, Fe_2O_3.

3.2. Heterogeneous Fenton's process (classical and HSPF)

In the heterogeneous Fenton process (Fig. 3a), 24% and 45% of color removals were achieved by using Fe(6%)/SBA-15 and Fe

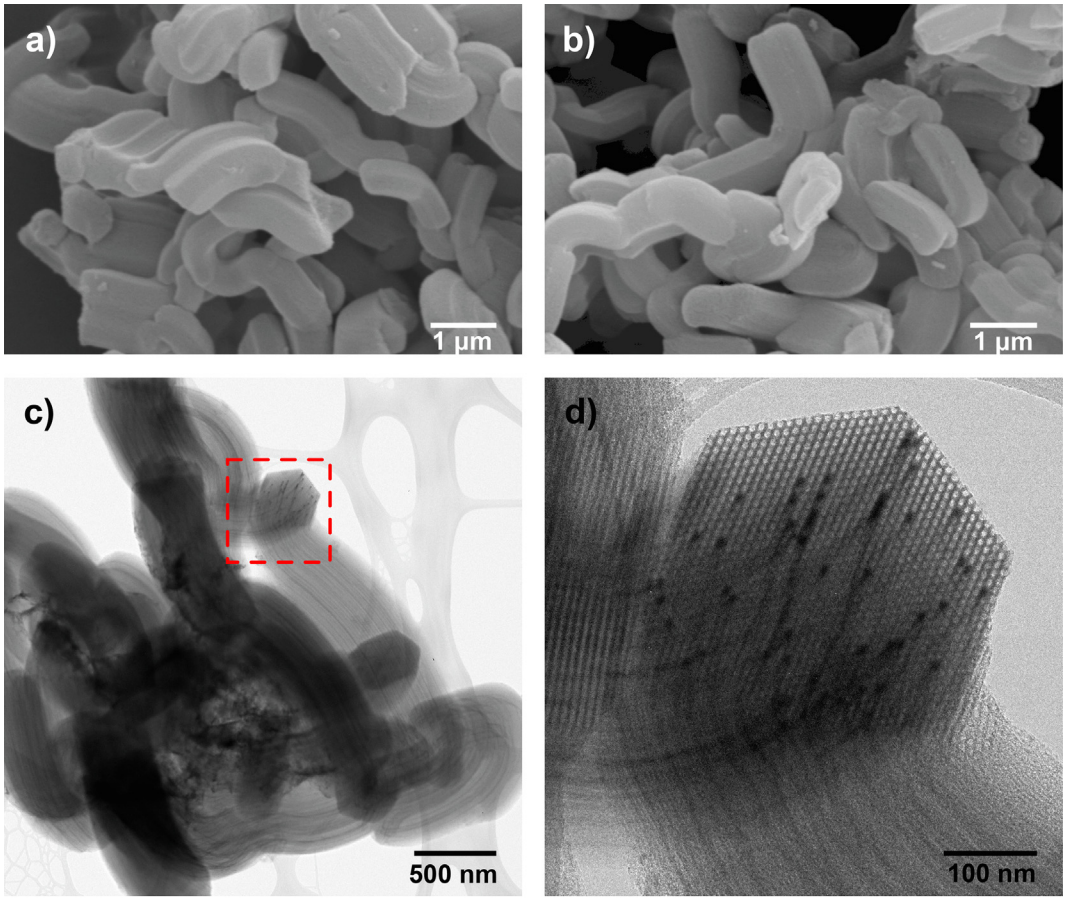

Fig. 1. SEM of a) SBA-15, b) Fe(10%)/SBA-15 at 15000 X, c) TEM image of the Fe(10%)/SBA-15 catalyst, and d) zoom of the highlighted zone.

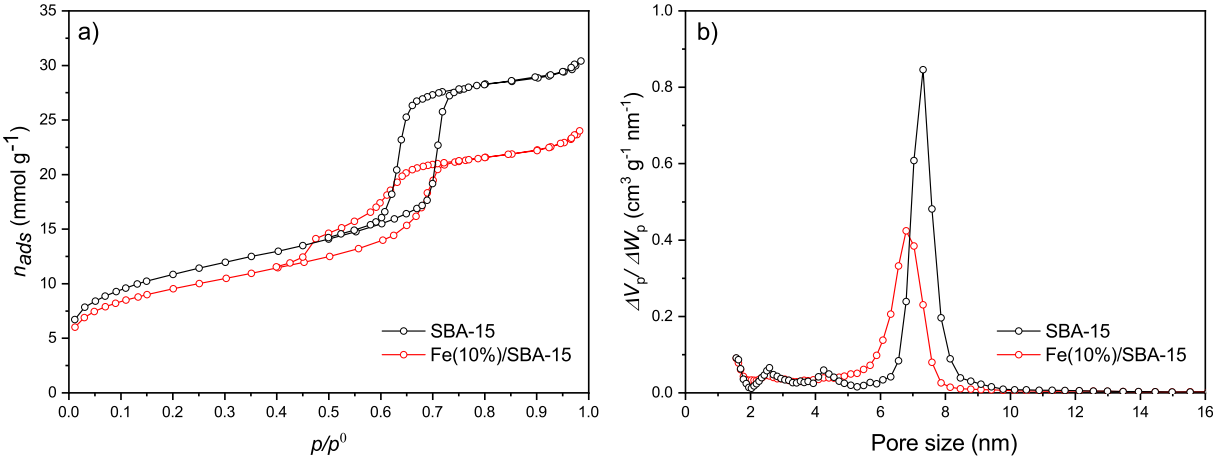

Fig. 2. a) N_2 adsorption–desorption isotherm at 77 K, and b) pore size distribution obtained from de adsorption data.

Table 1
Textural properties of the materials.

Material	S_{BET} (m^2 g^{-1})	V_t^1 (cm^3 g^{-1})	V_μ^2 (cm^3 g^{-1})	V_{MPP}^3 (cm^3 g^{-1})	w_p^4 (nm)
SBA-15	890	1.06	0.06	0.83	7.3
Fe(6%)/SBA-15	710	0.93	0.05	0.51	7.3
Fe(10%)/SBA-15	770	0.83	0.06	0.57	6.8

[1] Obtained by Gurvich's rule, [2–3] Obtained by α_s-plot, [4] Obtained from PSD.

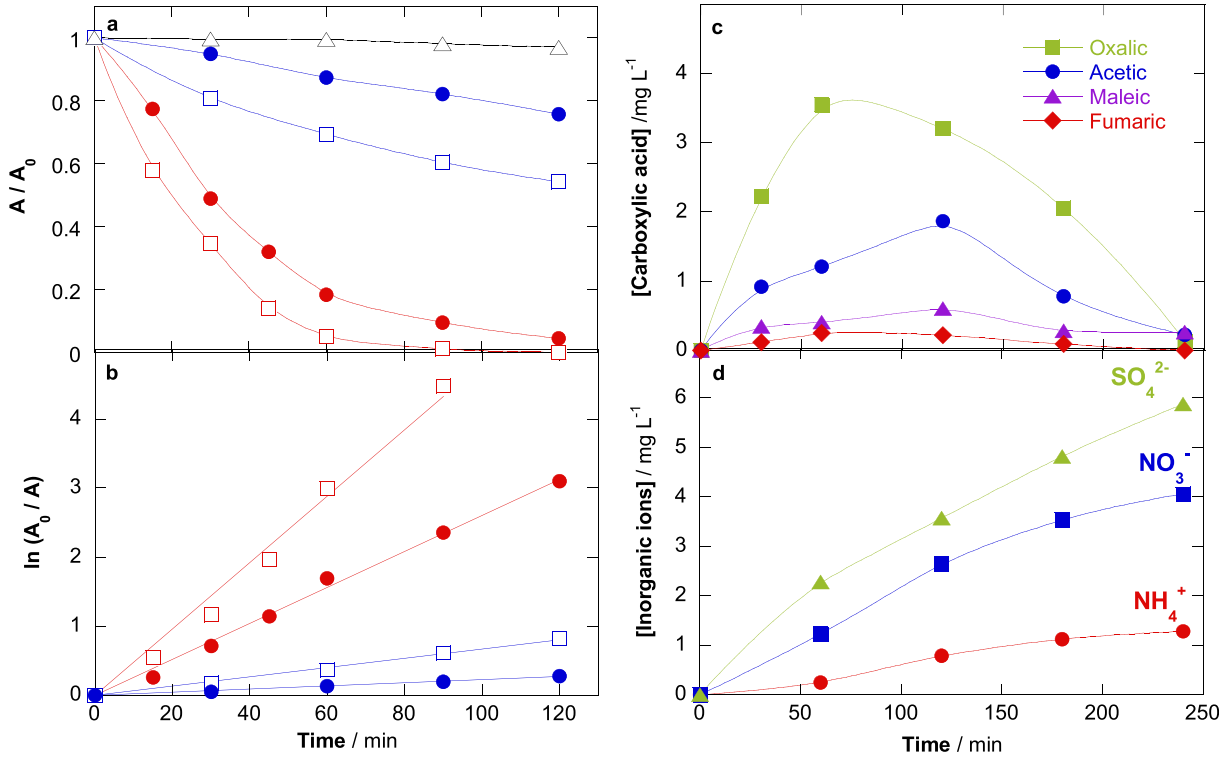

Fig. 3. Evaluation of the (a) discoloration with respective (b) pseudo first-order kinetics over time of 100 mL of 20 mg L^{-1} of MO with (Δ) SBA-15 (blank experiment), Fe/SBA-15 materials by using heterogeneous Fenton (●-6% Fe, □-10% Fe) and HSPF (●-6% Fe, □-10% F). Assessment of (c) carboxylic acids and (d) inorganic ions for HSPF with the Fe (10%)/SBA-15.

(10%)/SBA-15, respectively, after 120 min. In its turn, the use of HSPF revealed a faster discoloration in the same conditions. This statement is supported by the discoloration rate constants (k_{dec}) that fitted well with a pseudo-first-order kinetic model (Fig. 3b). In the heterogeneous Fenton process, initially the H_2O_2 is adsorbed on the surface of the catalyst in which iron is reduced through the Fenton-like reaction (1). After that, Fe^{2+} reacts with H_2O_2 producing ·OH radicals adsorbed at the active sites of the catalyst (2). It

seems that Fe(6%)/SBA-15 does not have enough active sites to promote efficiently the formation of ·OH from H_2O_2. Nevertheless, ·OH attacks the dye structure on the chromophore group (-N = N-), causing the discoloration solution. This process is slow due to Fe^{2+} recovery from Fe^{3+} step, resulting in the lower decomposition of H_2O_2 [13]. Conversely, the solar light radiation considerably increases the elimination rate, because it enhances the Fe^{2+} recovery and the generation ·OH (3), accelerating the discoloration process.

$$Fe^{3+}{}_{sites} + H_2O_2 \rightarrow Fe^{2+}{}_{sites} + {\cdot}O_2H + H^+ \quad (1)$$

$$Fe^{2+}{}_{sites} + H_2O_2 \rightarrow Fe^{3+}{}_{sites} + {\cdot}OH + OH^- \quad (2)$$

$$Fe^{3+}{}_{sites} + H_2O + h\nu \rightarrow Fe^{2+}{}_{sites} + {\cdot}OH + H^+ \quad (3)$$

After 240 min of reaction, 89% of COD removal was achieved for this experiment. An accumulation of short-chain linear carboxylic acids was detected over time (Fig. 3c) due to the cleavage of the dye-aromatic ring [14]. The conversion of initial S and N to inorganic species, such as SO_4^{2-}, NH_4^+ and NO_3^- was analyzed (Fig. 3d). A final SO_4^{2-} concentration of 5.87 mg L^{-1} was achieved due to the total conversion of the initial S into this specie. 1.28 mg L^{-1} of NH_4^+ and 4.06 mg L^{-1} of NO_3^- ions were also formed, corresponding to 38.7% and 35.6% of the initial N content, respectively.

4. Conclusions

The synthesized porous materials were tested towards MO degradation via two different Fenton approaches. In the case of heterogeneous Fenton, Fe/SBA-15 materials were not good catalysts to remove dye from water. However, when solar light irradiation was applied; these materials demonstrated to have potential photocatalytic activity to promote the production of oxidants in water, favoring the complete discoloration of dye in the effluent after 90 min and almost total degradation after 240 min. Short-chain linear carboxylic acids were detected. Initial S of the dye was totally converted to SO_4^{2-}, while initial N was partially converted to NH_4^+ and NO_3^-. Fe (10%)/SBA-15 demonstrated to be an efficient catalyst in the HSPF reactions. To assess the photocatalyst reutilization without losing photocatalytic activity, Fe(10%)/SBA-15 was recovered after usage and summited to several consecutive cycles of solutions degradation. After 5 cycles the catalyst attained identical percentages of MO solutions color removal, evidencing its potential applicability as photoactive material to wastewater treatment purposes. More experiments are in progress to test the usefulness of this kind of heterogeneous catalyst in other electrochemical applications, such as Electro-Fenton and PhotoElectro-Fenton [15].

CRediT authorship contribution statement

J.J. Arroyo-Gómez: Conceptualization, Methodology. **C.F. Toncón-Leal:** Formal analysis, Investigation. **A.J. dos Santos:** Writing - original draft, Conceptualization, Methodology. **M.S. Moreno:** Formal analysis, Investigation, Methodology. **K. Sapag:** Funding acquisition, Investigation. **C.A. Martínez-Huitle:** Supervision, Conceptualization, Funding acquisition.

Declaration of Competing Interest

The authors declare that they have no known competing financial interests or personal relationships that could have appeared to influence the work reported in this paper.

Acknowledgments

The authors thank to UNSL, FAPES (2014/50945-4) and CNPq (439344/2018-2) for the financial support.

Appendix A. Supplementary data

Supplementary data to this article can be found online at https://doi.org/10.1016/j.mlblux.2019.100034.

References

[1] A.N. Soon, B.H. Hameed, Desalination 269 (2011) 1–16.
[2] A.J. dos Santos, I. Sires, A.P.M. Alves, C.A. Martínez-Huitle, E. Brillas, Chemosphere 240 (2020) 124838.
[3] S. Foteinis, J.M. Monteagudo, A. Durán, E. Chatzisymeon, Sci. Total Environ. 612 (2018) 605–612.
[4] L.M.B. Batista, A.J. dos Santos, D.R. Silva, A.P.M. Alves, S. Garcia-Segura, C.A. Martinez-Huitle, Sci. Total Environ. 566–567 (2017) 79–86.
[5] X. Zhong, J. Barbier Jr., D. Duprez, H. Zhang, S. Royer, Appl. Catal. B 121–122 (2012) 123–134.
[6] T.B. Benzaquén, D.A. Barrera, P.M. Carraro, K. Sapag, O.M. Alfano, G.A. Eimer, Environ. Sci. Pollut. Res. 26 (2019) 4192–4201.
[7] C. Cornu, J.L. Bonardet, S. Casale, A. Davidson, S. Abramson, G. André, F. Porcher, I. Grčić, V. Tomasic, D. Vujevic, N. Koprivanac, J. Phys. Chem. C. 116 (2012) 3437–3448.
[8] S. Slichter, K. Sapag, M. Dennehy, M. Alvarez, J. Environ. Chem. Eng. 5 (2017) 5207–5214.
[9] M. Thommes, K. Kaneko, A.V. Neimark, J.P. Olivier, F. Rodriguez-Reinoso, J. Rouquerol, K.S.W. Sing, Pure Appl. Chem. 87 (2015) 1051–1069.
[10] D. Zhao, J. Feng, Q. Huo, N. Melosh, G. Fredrickson, B. Chmelka, G. Stucky, Science 279 (1998) 548–552.
[11] R. Cimino, K. Cychosz, M. Thommes, A. Neimark, Colloids Surf. A 437 (2013) 76–89.
[12] M. Kruk, M. Jaroniec, C.H. Ko, R. Ryoo, Chem. Mater. 12 (2000) 1961–1968.
[13] L. Chuan, Y. Liu, K. Li, J. Wen, S. Xing, Z. Ma, Y. Wu, Separ. Purif. Technol. 188 (2017) 105–111.
[14] A.J. dos Santos, C.A. Martínez-Huitle, I. Sires, E. Brillas, ChemElectroChem 5 (2018) 685–693.
[15] C.A. Martínez-Huitle, M. Panizza, Curr. Opin. Electrochem. 11 (2018) 62–71.